A Two-dimensional Analytical Model for Prediction of the Radiation Heat Transfer in Open-cell Metal Foams

Z. Jiang[a], K. Wang[a,*], H. Wu[b,*], Y. Wang[a], J. Du[a]

[a]Institute of Engineering Thermophysics, Chinese Academy of Sciences
Beijing, 100190, China.

[b]Institute of Engineering and Energy Technologies, School of Engineering and Computing,
University of the West of Scotland, Paisley, PA1 2BE, United Kingdom,

Abstract

In this article, anew simple two-dimensional (2D) explicit analytical model for the evaluation of the radiation heat transfer in highly porous open-cell metal foams is formulated and validated. A correction factor, *C*, is introduced to correct the deviation of the specific area for the purpose of simplification. The numerical results are compared with published experimental data and three-dimensional (3D) model proposed in previous works, and the present two-dimensional model is proved to be relatively accurate in estimating the radiative conductivity for all the investigated structures. In the current work, the effects of the control parameters, such as the number of order in the iterative procedure, solid emissivity, the temperature difference, shape of solid particle and correction factor on the predictions of radiation characteristics are well discussed.

Keywords: Modelling; Thermal radiation; Porous medium; Open-cell metal foam; Radiation heat transfer.

Nomenclature

a	side length [m]	X, Y	Cartesian coordinates [-]
A_{sf}	specific area [m^{-1}]	***Greek symbols***	
b	bottom face of the unit cell [-]	α_i	dimensional coefficient [-]
C	correction factor [-]	β_i	dimensional coefficient [-]
d	side length of the unit cell [m]	ε	solid emissivity[-]
d_f	diameter of strut [m]	ρ	solid reflectance [-]
d_p	characteristic cell size [m]	σ	Stefan-Boltzmann constant[W/ m^2K^4]
F	configuration factor [-]	ϕ	porosity [-]
H	foam sample thickness [m]	***Subscripts***	
i	sequence of the unit cell [-]	bt	void face b to void face t
J	irradiation from void face[W/m^2]	bj	void face b to solid particle j
k_r	radiative conductivity [W/m K]	c	cold side
l_b	length of bottom void face [m]	h	hot side
l_j	length of solid particle [m]	jk	solid particle j to solid particle k
l_s	length of side void face [m]	jt	solid particle j to void face t
l_t	length of top void face [m]	kt	solid particle k to void face t
N_c	total number of cells [-]	sj	void face s to solid particle j
q_r	radiation heat flux [W/m^2]	st	void face s to void face t
Q_r	irradiation [m s^{-2}]	***Superscripts***	
s	side face of the unit cell [-]	-	negative direction
t	top face of the unit cell [-]		
T	temperature [K]		

1. Introduction

Metal foams are extensively used for many industrial applications involving numerous technological fields over more than 50 years due to their attractive physical properties such as, high porosity, large specific surface, flow mixing enhancement, attractive stiffness properties and low cost [1]. Their averaged thermo-physical properties are also important for many applications, e.g., compact heat exchangers [2], solar receivers [3], and catalytic reactors [4]. The main characteristic of heat transfer in metal foams is dictated by the enhanced effective thermal conductivity (ETC). The ETC used to quantify the magnitude of heat conduction in metal foams is studied through model prediction [5-13], numerical simulation [14-16] and experimental research [16-18].

Previous publications reported on the thermal properties of metal foams at high temperature where conduction and radiation heat transfer may occur are relatively weak [19]. To overcome the experimental difficulties, Coquard et al. [20] proposed an innovative method to evaluate the conduction and radiation contribution in metal foams. They developed an identification method using thermograms obtained from laser-FLASH measurements to minimize the discrepancy between experimental and theoretical thermograms. Coquard et al. [19], afterwards, presented a detailed review on the radiation and conduction heat transfer from ambient to high temperature. They also proposed an analytical model for the real foams to predict the conduction and

radiation heat transfer at high temperature. Their predicted results agreed well with the experimental results [20].

Several studies have been devoted to the radiation heat transfer in metal foam [21-24]. Coquard et al. [21] modelled the radiation heat transfer in open cell metal foams and closed cell polymer foams utilizing two approaches, i.e., Homogeneous Phase Approach (HPA) and Multi-Phase Approach (MPA). The radiation heat transfer of these two types of foams was investigated using three-dimensional (3D) tomographic images. The calculated results were compared with the results of direct Monte Carlo (MC) simulations and the suitability of the two approaches was then evaluated. Tancrez et al. [22] developed a general method with direct identification of the radiation properties, i.e., absorption, scattering coefficients and phase function of porous medium using Monte Carlo (MC). This method was applied to both sets of Dispersed radius Overlapping Opaque Spheres (DOOS) in a transparent fluid phase and Dispersed radius Overlapping Transparent Spheres (DOTS) in an opaque solid phase. Zhao et al. [23] measured the ETC of metal foams with a range of pore sizes and porosities between 300 and 800 K. The radiative conductivity was decoupled from the equivalent conductivity due to conduction. As for the equivalent conductivity due to conduction contribution alone, the model proposed in [6] was used. At the same time, Zhao et al. [24] used the Rosseland equation to calculate the equivalent radiative conductivity based on the experimentally obtained spectral

67 transmittance and reflectance. The calculated results were found to be in satisfactory
68 agreement with the experimental data [23].
69 Although many significant results in the modelling radiation heat transfer of
70 open-cell metal foam have already been obtained, the aforementioned approaches are
71 not quite suitable for engineering applications. Thus, Zhao et al. [25] proposed an
72 explicit analytical model based on the simplified cubic structure. In this model, the
73 fundamental foam parameters and the emission and reflectance in metal foam
74 structure were considered to establish functional relationships between the structure
75 and the radiation characteristics of open-cell metal foams. The calculated equivalent
76 radiative conductivity showed that in general there was a good agreement between the
77 predicted and experimental data. Most recently, as an extension of the simplified
78 analytical approach of [25], Contento et al. [26] made further improvements by
79 recalculating the configuration factors that involved in the dimensionless coefficients
80 and a close agreement between predicted result and measured data was achieved. As
81 the same time, Contento et al. [27] developed a new radiative heat transfer model
82 based on a more realistic Lord Kelvin representation of open cell metal foams instead
83 of the simplified cubic structure using the same analytical approach. This explicit
84 simple approach that initially proposed by Zhao et al. [25] can be relatively suitable
85 for engineering applications.
86 Based on the brief literature review, it can be seen that much effort has been made
87 to develop models for estimation of radiation heat transfer in open-cell metal foam.

From an engineering perspective, however, due to the complex nature of the configuration factors for implementation in three-dimensional modelling, research on modelling radiation heat transfer has been far from complete. More effort needs to be made in this area. In this study, a newly simplified two-dimensional model is proposed and could serve as an efficient alternative to evaluate the radiative characteristics in porous open-cell metal foams for engineering applications. For the assessment of the new model, the comparisons between numerical predictions with experimental data [23] and previously proposed model [25] are carried out.

2. Model description

2.1. Structure simplification

The microstructure of typical open cell metal foam is shown in Fig. 1. Porous medium such as metal foams has a complex microstructure made up of solid ligaments and pores generally filled with fluid. In order to simplify the analysis of radiation heat transfer in metal foam, the microstructure can be assumed to be consisted of randomly oriented cells with characteristic size d_p which are mostly homogeneous in size and shape, whilst the solid of the metal foam can be treated as particles with simple geometry (circle, square and rectangle etc.) distributed in fluid zone regularly or randomly. In the current work, the connection of the solid phase of the metal foam can be neglected since the thermal radiation in metal foam mainly passes through the void due to the large porosity ($\phi \geqslant 90\%$) of metal foam.

Based on the above simplification, a new 2D structure with regularly distributed square particles with side length of a are selected to develop the analytical model for analysing the radiation heat transfer, as presented in Fig. 2(a). Since the structure is periodic, Fig. 2(b) shows the details of two neighbouring square unit cells. Within each cell, there are four quarters of solid particle at four corners which are labelled with *1-4* respectively. As for the four faces, two side faces are referred as *s*, whereas the top and bottom faces are represented by *t* and *b*. The relationship between d and measured d_p based on the same area is shown as:

$$d^2 = \frac{\pi}{4} d_p^2 \tag{1}$$

$$d = \frac{\sqrt{\pi}}{2} d_p \tag{2}$$

Then, a is obtained based on the porosity for the two-dimensional structure as:

$$\frac{4a^2}{d^2} = 1 - \phi \tag{3}$$

$$a = \sqrt{\frac{1-\phi}{4}} d \tag{4}$$

where ϕ is the porosity of the metal foam.

2.2. Assumptions

In order to simplify the heat transfer mechanism in open-cell metal foam, the following major assumptions were made in the derivations of the governing equations:

(i) The diffraction is neglected. The characteristic size of porous medium is considered as large compared to the heat radiation wavelengths.

(ii) The solid particles are assumed as grey and opaque since they are metallic. The void zone is considered as vacuum.

(iii) Surface of solid particles reflecting diffusely the incident radiation is assumed since surface roughness at 10μm scale is being taken into account [26].

(iv) Steady-state heat flow is assumed in a specific zone of the metal foam sandwiched between two plates with cold boundary temperature (T_c) for the top plate and hot boundary temperature (T_h) for the bottom plate. Sample is thermally insulated at side walls, which means that there exists a radiation heat flux in the positive *Y* direction.

(v) It is assumed that the radiation is decoupled from the conduction and the temperature varies linearly with *Y* direction [25].

(vi) Temperature difference within unit cell can be neglected since the porous foam sample is sufficiently thick. This means that each unit cell has a unique value of temperature in the same layer [26].

Other simplifications are described in the due course in the rest of the paper.

2.3. Mathematical formulations

2.3.1 Basic formulations

Based on the assumptions, the temperature difference between the two cells in adjacent planes in *Y* direction is represented by equation:

$$\Delta T = \frac{T_h - T_c}{N_c} \tag{5}$$

where ΔT is the temperature difference between two cells in adjacent planes, N_c

denotes the total number of cells in *Y* direction which is given by:

$$N_c = \frac{H}{d} \tag{6}$$

where *H* is the thickness of the porous medium sample. The temperature of the *i*th (i=1,2,3… N_c) cell is:

$$T[i] = T_h - (i-1)\Delta T \tag{7}$$

Thus, the radiative conductivity k_r can be obtained by:

$$k_r = \frac{q_{r,net}}{(T_h - T_c)/H} \tag{8}$$

where $q_{r,net}$ is the net radiation heat flux.

The net radiation heat flux $q_{r,net}$ will be calculated based on the top void face *t* of the *i*th cell. Since the radiation heat fluxes in both directions are not identical, the net radiation heat flux can be mathematically expressed by the following equation:

$$q_{r,net} = q_r - q_r^- \tag{9}$$

where q_r is the radiation heat flux in the positive *Y* direction and q_r^- is the radiation heat flux in the negative *Y* direction, respectively.

2.3.2 Derivation

Firstly, radiation in the positive *Y* direction will be analysed, as radiation in the negative *Y* direction is familiar with that in positive *Y* direction. As shown in Fig. 2(b), the total irradiation on the void face *t* of the *i*th cell includes both the emission and reflectance from the solid particles *1-4* to the void faces *s*, *b*. The total irradiation Q_r on *t* is given by:

$$Q_r = (Q_r)_{emission} + (Q_r)_{reflectance} \tag{10}$$

where,

$$(Q_r)_{emission} = \sum_{j=1}^{4} l_j F_{jt} \cdot \varepsilon\sigma T^4 + l_b F_{bt} J_b + 2 l_s F_{st} J_s \quad (11)$$

where $l_j(j=1,2,3,4)$ is the length of the jth solid particle within a unit cell, ε is the solid emissivity, σ is Stefan-Boltzmann constant equal to $5.669\text{x}10^{-8}$ W/m^{2}K^4, T is the temperature of the unit cell, l_b and J_b are the length and irradiation of the void face b, l_s and J_s are the length and irradiation of the void faces, F is the configuration factor.

The three terms on the right side of Eq. (11) are the emission on the void face t from four solid particles in four corners, bottom void face b and side void faces s, respectively.

$$(Q_r)_{reflectance} = \sum_{j=1}^{4} \sum_{k=1, j\neq k}^{4} \rho l_j F_{jk} F_{kt} \cdot \varepsilon\sigma T^4 + \sum_{j=1}^{4} \rho l_b F_{bj} F_{jt} J_b + 2\sum_{j=1}^{4} \rho l_s F_{sj} F_{jt} J_s \quad (12)$$

where $\rho=1-\varepsilon$ is the solid reflectivity. Similarly, the three terms on the right side of Eq. (12) represent the reflectance of incident radiation on the solid particles from each other, bottom void face and two side faces, respectively.

Considering the model is two-dimensional, the unit of Q is W/m.

In the current study, the configuration factors can be analysed geometrically. The following formulations are used:

$$F_{12} = F_{21} = F_{13} = F_{31} = F_{34} = F_{43} = F_{24} = F_{42} = F_1 \quad (13)$$

$$F_{14} = F_{41} = F_{23} = F_{32} = F_2 \quad (14)$$

$$F_{1t} = F_{2t} = F_3 \quad (15)$$

$$F_{3t} = F_{4t} = F_4 \quad (16)$$

$$l_1 = l_2 = l_3 = l_4 \tag{17}$$

$$l_t = l_b = l_s \tag{18}$$

$$F_{s1} = F_{s3} = F_{b3} = F_{b4} = \frac{l_1}{l_s} F_3 \tag{19}$$

$$F_{s2} = F_{s4} = F_{b1} = F_{b2} = \frac{l_1}{l_s} F_4 \tag{20}$$

where l_t is the length of the top void face in the unit cell.

Radiation in the positive Y direction is given by:

$$q_r = \frac{Q_r}{l_t} \tag{21}$$

Substitute Eqs. (13-20) to Eq. (21), the radiation in the positive Y direction can be expressed in the following manner:

$$q_r = \frac{Q_r}{l_t} = \frac{l_1}{l_t}(2 + 4\rho F_1 + 2\rho F_2)(F_3 + F_4)\varepsilon\sigma T^4$$

$$+ (F_{bt} + 4\frac{l_1}{l_t}\rho F_3 F_4) J_b + \left[2F_{st} + 2\frac{l_1}{l_t}\rho (F_3 + F_4)^2 \right] J_s \tag{22}$$

For the simplification of Eq. (22), dimensionless coefficients β_1, β_2, β_3 are introduced and defined as:

$$\beta_1 = l_1(2 + 4\rho F_1 + 2\rho F_2)(F_3 + F_4) / l_t \tag{23}$$

$$\beta_2 = F_{bt} + 4 l_1 \rho F_3 F / l_t \tag{24}$$

$$\beta_3 = 2F_{st} + 2 l_1 \rho (F_3 + F_4)^2 / l_t \tag{25}$$

Thus, Eq. (22) can be further reduced to:

$$q_r = \beta_1 \varepsilon\sigma T^4 + \beta_2 J_b + \beta_3 J_s \tag{26}$$

In order to calculate the radiation in the positive Y direction q_r, J_b and J_s which are in

the right side of Eq. (26) need to be calculated first. Similarly, the irradiation from void face *s*, J_s can be analyzed

$$J_s = \frac{l_1}{l_s}(2+4\rho F_1+2\rho F_2)(F_3+F_4)\varepsilon\sigma T^4$$

$$+(F_{bt}+4\frac{l_1}{l_s}\rho F_3F_4)J_s+\left[F_{st}+\frac{l_1}{l_s}\rho(F_3+F_4)^2\right]J_b \quad (27)$$

The quantity of J_s can be calculated from Eq. (27) which is written as following equation:

$$J_s = \frac{l_1(2+4\rho F_1+2\rho F_2)(F_3+F_4)/l_s}{1-F_{bt}-4l_1\rho F_3F/l_s}\varepsilon\sigma T^4+\frac{2F_{st}+2l_1\rho(F_3+F_4)^2/l_s}{1-F_{bt}-4l_1\rho F_3F/l_s}J_b \quad (28)$$

Eq. (28) can be further written as:

$$J_s = \alpha_1\varepsilon\sigma T^4+\alpha_2 J_b \quad (29)$$

where α_1 and α_2 are the dimensionless coefficients, defined as:

$$\alpha_1 = \frac{l_1(2+4\rho F_1+2\rho F_2)(F_3+F_4)/l_s}{1-F_{bt}-4l_1\rho F_3F/l_s} \quad (30)$$

$$\alpha_2 = \frac{2F_{st}+2l_1\rho(F_3+F_4)^2/l_s}{1-F_{bt}-4l_1\rho F_3F/l_s} \quad (31)$$

Substitute Eq. (29) to Eq. (26) lead to:

$$q_r = (\beta_1+\beta_3\alpha_1)\varepsilon\sigma T^4+(\beta_2+\beta_3\alpha_2)J_b \quad (32)$$

2.3.3 Iteration process

For the convenience of iteration process, q_r, T, J_b of the *i*th unit cell can be rewritten as $q_r[i]$, $T[i]$, $J_b[i]$, thus, Eq.(32) can be rewritten as:

$$q_r[i] = (\beta_1+\beta_3\alpha_1)\varepsilon\sigma(T[i])^4+(\beta_2+\beta_3\alpha_2)J_b[i] \quad (33)$$

As the bottom face *b* of the *i*th unit cell is the top face of the (*i-1*)th unit cell.

Therefore, the Eq. (33) can be expressed as:

$$q_r[i] = (\beta_1 + \beta_3\alpha_1)\varepsilon\sigma(T[i])^4 + (\beta_2 + \beta_3\alpha_2)q_r[i-1] \quad (34)$$

Similarly,

$$q_r[i-1] = (\beta_1 + \beta_3\alpha_1)\varepsilon\sigma(T[i-1])^4 + (\beta_2 + \beta_3\alpha_2)q_r[i-2] \quad (35)$$

$$q_r[i-2] = (\beta_1 + \beta_3\alpha_1)\varepsilon\sigma(T[i-2])^4 + (\beta_2 + \beta_3\alpha_2)q_r[i-3] \quad (36)$$

…

where the bottom face of the first unit cell is the bottom boundary of the porous medium sample with the temperature T_h, thus:

$$q_r[1] = (\beta_1 + \beta_3\alpha_1)\varepsilon\sigma(T[i-2])^4 + (\beta_2 + \beta_3\alpha_2)\varepsilon\sigma T_h^{\,4} \quad (37)$$

Thus, the quantity of $q_r[i]$ can be calculated implementing an iterative procedure from the boundary.

In the case of the radiation flux in the negative y direction, it can similarly be written as:

$$q_r^-[i] = (\beta_1 + \beta_3\alpha_1)\varepsilon\sigma(T[i+1])^4 + (\beta_2 + \beta_3\alpha_2)J_b^-[i] \quad (38)$$

where $J_b^-[i]$ is the irradiation on void face *t* of *i*th unit cell from the top void face of the (*i+1*)th unit cell, as shown in Fig. 2(b).

Similarly,

$$q_r^-[i] = (\beta_1 + \beta_3\alpha_1)\varepsilon\sigma(T[i+1])^4 + (\beta_2 + \beta_3\alpha_2)q_r^-[i+1] \quad (39)$$

$$q_r^-[i+1] = (\beta_1 + \beta_3\alpha_1)\varepsilon\sigma(T[i+2])^4 + (\beta_2 + \beta_3\alpha_2)q_r^-[i+2] \quad (40)$$

…

$$q_r^-[N_c] = \varepsilon\sigma T_c^{\,4} \quad (41)$$

The determination of $q_r^-[i]$ is the same as that of $q_r[i]$. Then $q_{r,net}$ can be calculated by Eq. (9). Consequently, the equivalent radiative conductivity is determined by Eq. (8).

3. Determination of coefficients

In the analytical solution of the equivalent radiative conductivity, the dimensionless coefficients, i.e., β_1, β_2, β_3 and α_1, α_2 need to be determined. As previously mentioned, the coefficients are the functions of the configuration factors, geometric parameters and the solid reflectance according to Eqs. (23-35) and Eqs. (30,31). In order to determine these coefficients, the configuration factors, F_1, F_2, F_3, F_4, F_{bt} and F_{st}, should be firstly determined. The crossed strings method is utilized to calculate the configuration factors for a two-dimensional geometric structure with known geometric parameters of the unit cell.

As for the solid reflectance, it is recognized that the solid reflectance is related to the emissivity ($\rho+\varepsilon=1$ for opaque material). However, the emissivity of a solid material depends on many other factors such as temperature and orientation. The influence of the emissivity on the radiation heat transfer is discussed in the next section.

4. Results and discussion

4.1. Model validation

In the current work, the validation of the model is based on the FeCrAlY (Fe 75%, Cr 20%, Al 5%, Y 2%) metallic foam produced via the sintering route which is

studied by Zhao et al. [23]and the test conditions employed for the current simulation are listed in Table 1. Due to the fact that the real values of the geometric parameters of the metal foam usually are different from that supplied by manufacturers, the measured values instead of the nominal values will be considered. The currently developed model will be evaluated through the comparison of the equivalent radiative conductivity between the experimental data [23] and previous numerical results [25,26].

The predicted results for all samples are shown in Figs. 3-6. It is clearly seen that there is a large deviation between experimental data and predicted results for all samples. It reveals that the currently developed model does not fully show the geometrical characteristics of three-dimensional structure of metal foam. Thus, this model needs to be corrected and modified.

In the simplified 2D model, the specific surface area can be defined as the ratio of the total side length of solid particles and the area:

$$A_{sf,2D} = \frac{8a}{d^2} \tag{42}$$

As for 3D structure of metal foam, following reference [28], the specific surface area is defined as:

$$A_{sf,3D} = \frac{3\pi d_f [1 - e^{-(1-\phi)/0.04}]}{(0.59 d_p)^2} \tag{43}$$

where d_f is diameter of the strut. It is noted that the specific surface area in the present 2D model is different from that in 3D structure, which results in the deviation of the emission from solid particles in the calculation of radiation. In order to reduce

this deviation, a correction factor (*C)* is introduced to correct the emission from solid particles, which is defined as:

$$C = \frac{A_{sf,3D}}{A_{sf,2D}}$$

$$= \frac{3\pi d_f [1 - e^{-(1-\phi)/0.04}] d^2}{8a(0.59 d_p)^2}$$

$$= 1.0773\pi^{2.5}(1-\phi)^{-0.5}[1 - e^{-(1-\phi)/0.04}]\frac{d_f}{d_p} \quad (44)$$

Thus, the previous analysis needs to be reconsidered. The proposed correction factor *C* is added into the item of emission radiation in Eqs. (11-12), then Eqs. (11-12) are rewritten as:

$$(Q_r)_{emission} = \sum_{j=1}^{4} C l_j F_{jt} \cdot \varepsilon\sigma T^4 + l_b F_{bt} J_b + 2 l_s F_{st} J_s \quad (45)$$

$$(Q_r)_{reflectance} = \sum_{j=1}^{4} \sum_{k=1, j\neq k}^{4} C\rho l_j F_{jk} F_{kt} \cdot \varepsilon\sigma T^4 + \sum_{j=1}^{4} \rho l_b F_{bj} F_{jt} J_b + 2\sum_{j=1}^{4} \rho l_s F_{sj} F_{jt} J_s \quad (46)$$

The rest of the derivation is similar to the previous analysis. The same iteration is carried out to obtain the radiative conductivity. Firstly, the effect of the correction is observed. Fig. 7 shows the predicted radiative conductivity with and without the correction factor for S1. It can be seen that the effect of correction is significant. It reveals that, in the process of simplification, the geometrical characteristics needs to stay consistent to ensure the validity of simplified model.

Figs. 8-11 show the comparison of the radiative conductivity versus temperature at different pores per inch (PPI) and porosity between the present predicted results of corrected model and experimental data [23] as well as previously numerical

results[25,26]. The results in Figs. 8-11 clearly show that the proposed model and model from reference [26] perform well in predicting the experimental data in all cases, while the initial model proposed by Zhao et al. [25] did not perform well for the cases of S2 and S4. Percent differences between the predicted results and the experimental data are reported in Table 2. And it is noted that there may have been a slight over-estimation or under-estimation of the radiative conductivity. This could be mainly due to the fact that the current model assumes uniform distribution of the solid particles in the porous media and uses the average particle diameter whereas in the real case the particle size is within a certain range. Despite this, it can be seen that in general there is a good agreement between the currently predicted and the experimental data.

Then the effects of the control parameters such as, the number of the orders, the solid emissivity, temperature gradient, and the geometry on the radiative conductivity will be examined in detail.

4.2. Effect of number of orders

As analyzed in section 2, the radiative conductivity is determined by implementing an iterative procedure which takes into account the irradiation from other unit cells up to the ones in contact with the boundaries. We define that the model has first-order accuracy if the *(i-1), i, (i+1), (i+2)*th unit cells are reserved which implies that the *i*th cell and *(i+1)*th cell share the face *t* that only accounts for the contributions from the adjacent neighbouring cells(*(i-1)*th, *(i+2)*th) in both directions. Geometrically, the

face *t* is the central face within these four cells along y direction. Thus, the bottom face of the *(i-1)*th cell and the top face of *(i+2)*th cell are boundaries. Similarly, for second-order accuracy, one more unit cell in both directions is included in the calculation. For the other numbers of the orders, they can be defined in a same principle. Fig.12 shows that the radiative conductivity of sample 1varies with the number of the order at two different temperatures, i.e.550K and , 750K at a solid emissivity of 0.6It reveals that the numbers of cells above and below the central face need to be considered to obtain the stable values of radiative conductivity. Thus, in order to stabilize the calculated values of the radiative conductivity, the number of orders of 25is used for the current model.

4.3. Effect of the solid emissivity

As previously mentioned, the effect of the solid emissivity on the radiative conductivity needs to be addressed. Generally, the emissivity of the steel varies between 0.3 and 0.8[29]. Fig.13 shows the effect of the solid emissivity on the values of radiative conductivity at two temperatures of 550 K and 750 K. It is clearly seen that the value of the radiative conductivity increases with increasing solid emissivity even though a large emissivity can lead to a smaller reflectance. It reveals that the proportion of the emission in total radiation is relatively large. In addition, the effect of the solid emissivity on the radiative conductivity is significant at temperature of 750 K, while it is relatively mild at temperature of 550 K. The reason could be that the emitting radiation is in proportion to the biquadrate of temperature. For the

purpose of comparison, a solid emissivity of 0.6 is assumed in present work, which is consistent with the previous study of [25] and [26].

4.4. Effect of temperature gradient

For a fixed thickness with the same mean temperature, the effect of the temperature difference on the predicted radiative conductivity at fixed temperature of 750 K is shown in Fig. 14. A specific mean temperature can be determined in different temperature difference between the top and bottom boundaries of the foam samples. It can also be concluded from Fig. 14 that the radiative conductivity is not sensitive to the temperature difference. In the current model, therefore, a 10 K temperature difference is used for the iterative procedure.

4.6. Effect of geometry

As mentioned in Section 2.1, the shape of the solid particles can be other simple geometries. For example, two shapes, such as circle, rhombus are assumed based on the same porosity and characteristic size to investigate the effect of shape of solid particles as seen in Fig. 15. The calculations are shown in Fig. 16 for the case of S1. It can be seen that shape of the solid particles has insignificant effect on the thermal radiation in the present model. It is noted that different shapes of the solid particles may lead to different geometry structure for the present simplified 2D model, which implies that the configuration factors may be different. However, due to the large porosity of metal foam, the influence of different structures is insignificant in general.

Fig. 17 demonstrates the variation of radiative conductivity with the change of the PPI for the same porosity of 95%.For comparison purposes, two PPI are used i.e. 30 and 60. Comparison shows that the radiative conductivity increases monotonously with decreasing PPI at the same temperature, such a result is due to the smaller PPI results in a bigger pore size. And the bigger pore size would lead to a large "penetration thickness" which implies that more heat can be directly transferred by thermal radiation to a deeper thickness of the foam before it decays to a lower level [25].

5. Conclusions

A newly developed two-dimensional model is employed for the calculation of the radiation heat transfer in highly porous open-cell metal foams and comparing these results with available experimental data as well as three-dimensional numerical solution proposed in the previous work. A correction factor, *C*, is introduced for the correction of the deviation of the specific area between simplified two-dimensional structure and three-dimensional structure. The results demonstrated that using a two-dimensional analytical model instead of a three-dimensional approach leads to a relatively minor discrepancy. Besides, the calculation is simpler than the three-dimensional model because of the simpler determination of configuration factors and coefficients due to the nature of two-dimensional structure, which is significant for engineering applications. The effect of the solid emissivity on the radiative conductivity is more significant at higher temperature. The radiative

conductivity is not sensitive to the temperature difference during the iterative procedure. The effect of the shape of the solid particle is observed and it is relatively small. It is found that the samples with smaller PPI could lead to a higher value of radiative conductivity. In addition, the correction factor *C* is found to be significant for the present model. Overall, the biggest advantage of the proposed two-dimensional model is its simplicity and convenience of calculation with good accuracy compared to the previous three-dimensional model. However, the present model is only suitable for vacuum condition. Future work needs to be done to investigate the thermal radiation in metal foam in atmospheric pressure. Besides, more experimental data of different metal foams (material, PPI, porosity etc.) are needed in order to validate the present model.

Acknowledgements

The authors would like to acknowledge the financial support from National Natural Science Foundation of China (No. 51206164).

References

[1] C. Y. Zhao, Review on thermal transport in high porosity cellular metal foams with open cells, Int. J. Heat Mass Transfer, 55(13-14) (2012) 3618-3632.

[2] S. Y. Kim, J. W. Paek and B. H. Kang, Flow and heat transfer correlations for porous fin in a plate-fin heat exchanger, J Heat Trans- ASME, 122(3) (2000) 572-578.

[3] C. Albanakis, D. Missirlis, N. Michailidis, K. Yakinthos, A. Goulas, H. Omar, D. Tsipas and B. Granier, Experimental analysis of the pressure drop and heat transfer through metal foams used as volumetric receivers under concentrated solar radiation, Exp. Therm Fluid Sci., 33(2) (2009) 246-252.

[4] X. H. Yu, Z. Z. Wen, Y. Lin, S. T. Tu, Z. D. Wang and J. Y. Yan, Intensification of biodiesel synthesis using metal foam reactors, Fuel, 89(11) (2010) 3450-3456.

[5] A. Bhattacharya, V. V. Calmidi and R. L. Mahajan, Thermophysical properties of high porosity metal foams, Int. J. Heat Mass Transfer, 45(5) (2002) 1017-1031.

[6] K. Boomsma and D. Poulikakos, On the effective thermal conductivity of a three-dimensionally structured fluid-saturated metal foam, Int. J. Heat Mass Transfer, 44(4) (2001) 827-836.

[7] V. V. Calmidi and R. L. Mahajan, The effective thermal conductivity of high porosity fibrous metal foams, J Heat Trans-T Asme, 121(2) (1999) 466-471.

[8] Z. Dai, K. Nawaz, Y. G. Park, J. Bock and A. M. Jacobi, Correcting and extending the Boomsma-Poulikakos effective thermal conductivity model for three-dimensional, fluid-saturated metal foams, Int. Commun. Heat Mass Transfer, 37(6) (2010) 575-580.

[9] M. A. A. Mendes, S. Ray and D. Trimis, A simple and efficient method for the evaluation of effective thermal conductivity of open-cell foam-like structures, Int. J. Heat Mass Transfer, 66 (2013) 412-422.

435 [10] M. A. A. Mendes, S. Ray and D. Trimis, An improved model for the effective
436 thermal conductivity of open-cell porous foams, Int. J. Heat Mass Transfer, 75
437 (2014) 224-230.
438 [11] J. W. Paek, B. H. Kang, S. Y. Kim and J. M. Hyun, Effective thermal
439 conductivity and permeability of aluminum foam materials, Int. J.
440 Thermophysics, 21(2) (2000) 453-464.
441 [12] R. Singh and H. S. Kasana, Computational aspects of effective thermal
442 conductivity of highly porous metal foams, Appl. Therm. Eng., 24(13) (2004)
443 1841-1849.
444 [13] B. Dietrich, G. Schell, E. C. Bucharsky, R. Oberacker, M. J. Hoffmann, W.
445 Schabel, M. Kind and H. Martin, Determination of the thermal properties of
446 ceramic sponges, Int. J. Heat Mass Transfer, 53(1-3) (2010) 198-205.
447 [14] R. Coquard and D. Baillis, Numerical investigation of conductive heat transfer in
448 high-porosity foams, AcMat, 57(18) (2009) 5466-5479.
449 [15] P. Kumar and F. Topin, Simultaneous determination of intrinsic solid phase
450 conductivity and effective thermal conductivity of Kelvin like foams, Appl.
451 Therm. Eng., 71(1) (2014) 536-547.
452 [16] M. A. A. Mendes, V. Skibina, P. Talukdar, R. Wulf, U. Gross, D. Trimis and S.
453 Ray, Experimental validation of simplified conduction–radiation models for
454 evaluation of Effective Thermal Conductivity of open-cell metal foams at high
455 temperatures, Int. J. Heat Mass Transfer, 78 (2014) 112-120.

[17] E. Solorzano, M. Hirschmann, M. A. Rodriguez-Perez, C. Korner and J. A. de Saja, Thermal conductivity of AZ91 magnesium integral foams measured by the Transient Plane Source method, MatL, 62(24) (2008) 3960-3962.

[18] R. Wulf, M. A. A. Mendes, V. Skibina, A. Al-Zoubi, D. Trimis, S. Ray and U. Gross, Experimental and numerical determination of effective thermal conductivity of open cell FeCrAl-alloy metal foams, Int. J. Thermal Sciences, 86 (2014) 95-103.

[19] R. Coquard, D. Rochais and D. Baillis, Conductive and Radiative Heat Transfer in Ceramic and Metal Foams at Fire Temperatures, Fire Technol., 48(3) (2010) 699-732.

[20] R. Coquard, D. Rochais and D. Baillis, Experimental investigations of the coupled conductive and radiative heat transfer in metallic/ceramic foams, Int. J. Heat Mass Transfer, 52(21-22) (2009) 4907-4918.

[21] R. Coquard, D. Baillis and J. Randrianalisoa, Homogeneous phase and multi-phase approaches for modeling radiative transfer in foams, Int. J. Thermal Sciences, 50(9) (2011) 1648-1663.

[22] M. Tancrez and J. Taine, Direct identification of absorption and scattering coefficients and phase function of a porous medium by a Monte Carlo technique, Int. J. Heat Mass Transfer, 47(2) (2004) 373-383.

[23] C. Y. Zhao, T. J. Lu, H. P. Hodson and J. D. Jackson, The temperature dependence of effective thermal conductivity of open-celled steel alloy foams, Mat Sci Eng a-Struct, 367(1-2) (2004) 123-131.

[24] C. Y. Zhao, T. J. Lu and H. P. Hodson, Thermal radiation in ultralight metal foams with open cells, Int. J. Heat Mass Transfer, 47(14-16) (2004) 2927-2939.

[25] C. Y. Zhao, S. A. Tassou and T. J. Lu, Analytical considerations of thermal radiation in cellular metal foams with open cells, Int. J. Heat Mass Transfer, 51(3-4) (2008) 929-940.

[26] G. Contento, M. Oliviero, N. Bianco and V. Naso, Prediction of radiative heat transfer in metallic foams, Int. J. Thermal Sciences, 76 (2014) 147-154.

[27] G. Contento, M. Oliviero, N. Bianco and V. Naso, The prediction of radiation heat transfer in open cell metal foams by a model based on the Lord Kelvin representation, Int. J. Heat Mass Transfer, 76 (2014) 499-508.

[28] V.V. Calmidi, R.L. Mahajan, Forced convection in high porositymetal foams, ASME J. Heat Transfer 122 (2000) 557 – 565.

[29] M. L. Hunt and C. L. Tien, Effects of Thermal Dispersion on Forced-Convection in Fibrous Media, Int. J. Heat Mass Transfer, 31(2) (1988) 301-309.

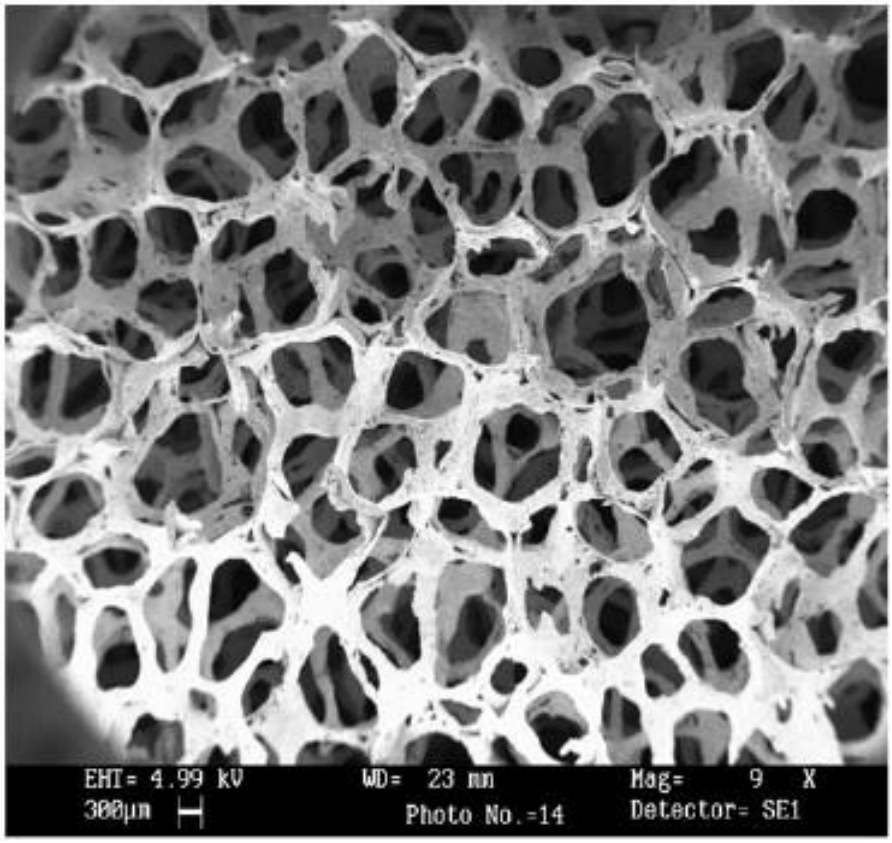

Fig. 1. Typical open-cell metallic foam morphology [25].

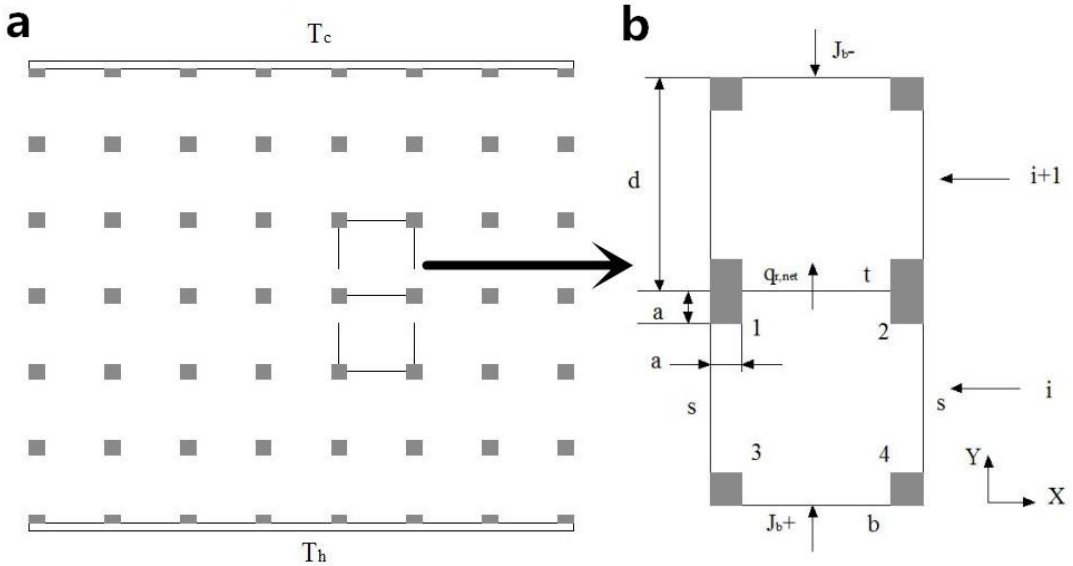

Fig. 2. (a) Two-dimensional idealized structure of porous medium; (b) Model foam structure and notations.

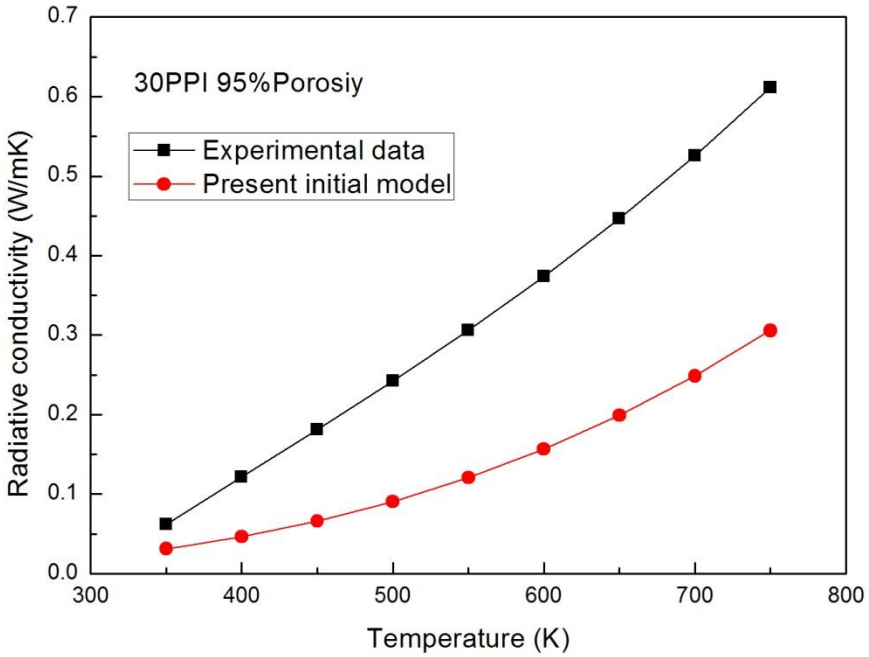

Fig. 3. Comparison between experimental data and predicted results of present initial model for S1.

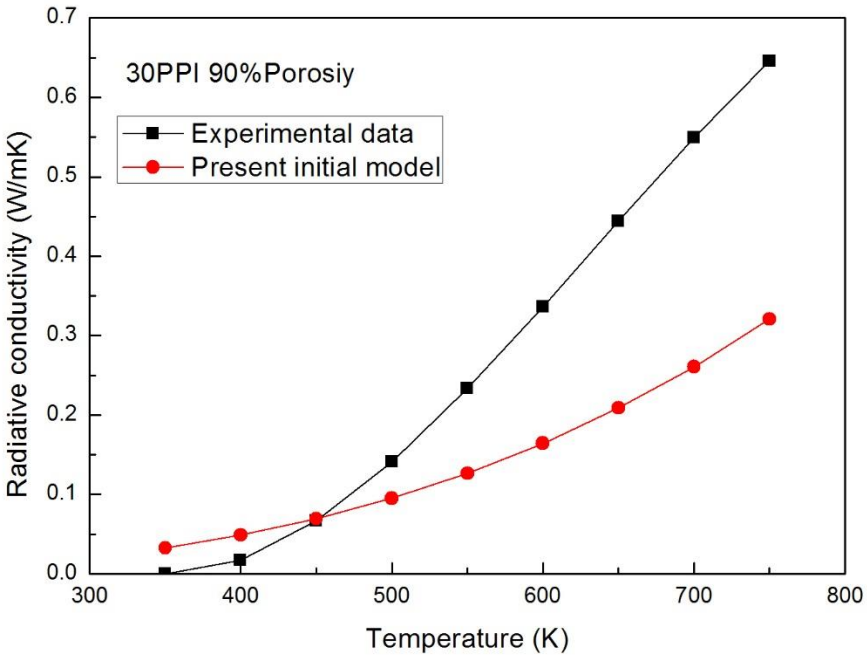

Fig. 4. Comparison between experimental data and predicted results of present initial model for S2.

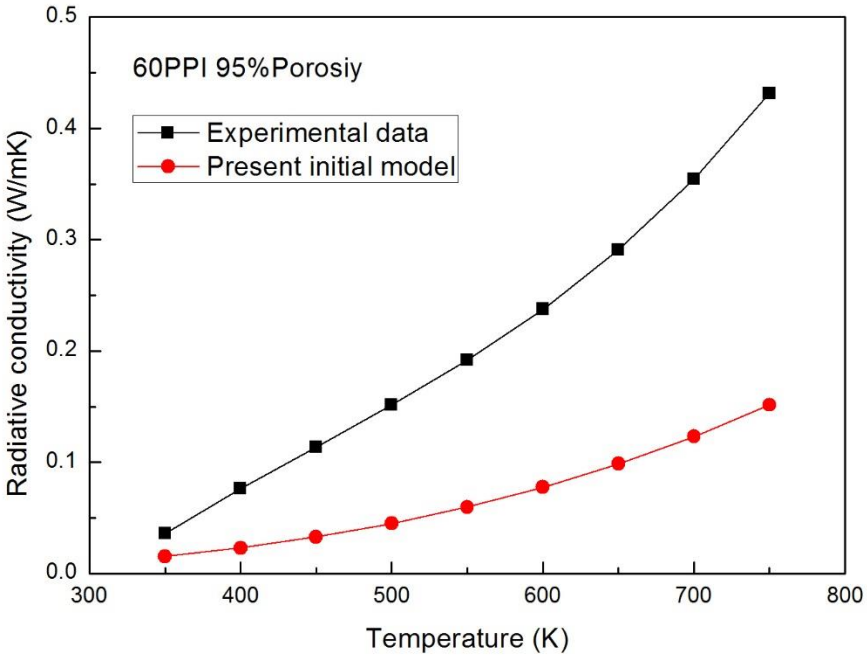

508

509 **Fig. 5.** Comparison between experimental data and predicted results of present initial
510 model for S3.

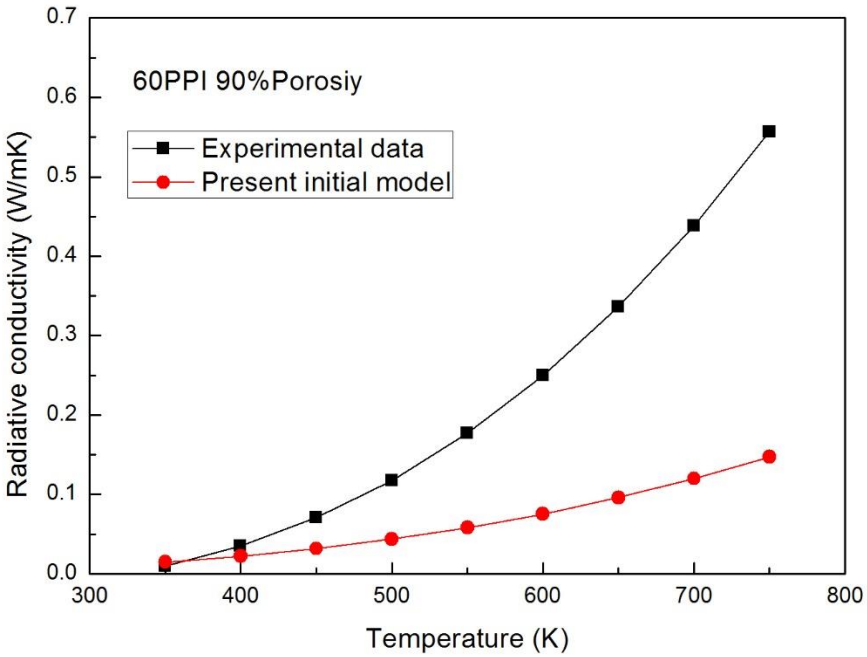

511

512 **Fig. 6.** Comparison between experimental data and predicted results of present initial
513 model for S4.

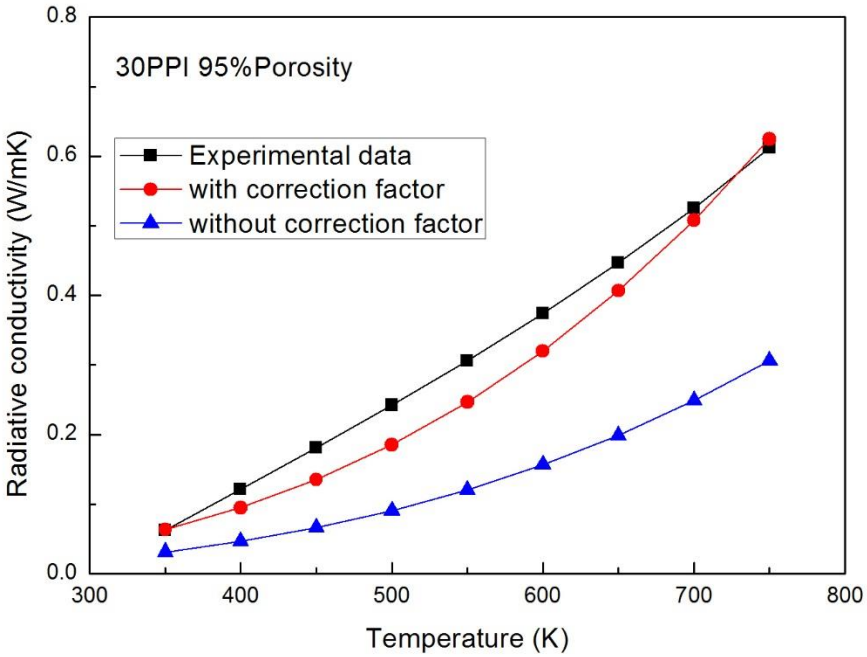

514

515 **Fig. 7.** Effect of correction factor on radiative conductivity for S1.

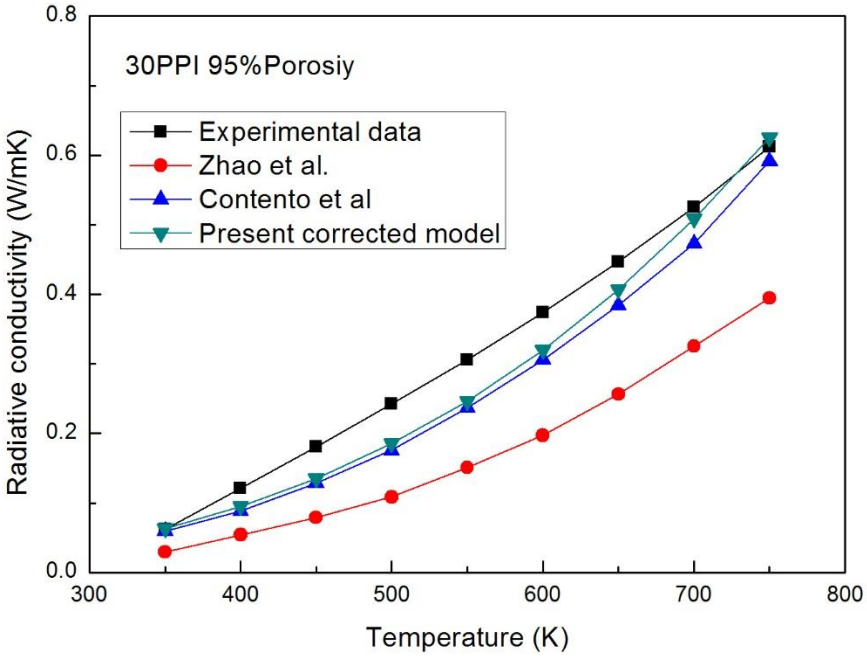

516

517 **Fig. 8.** Comparison between predicted results of present corrected model and
518 experimental data, results of previous 3D models for S1.

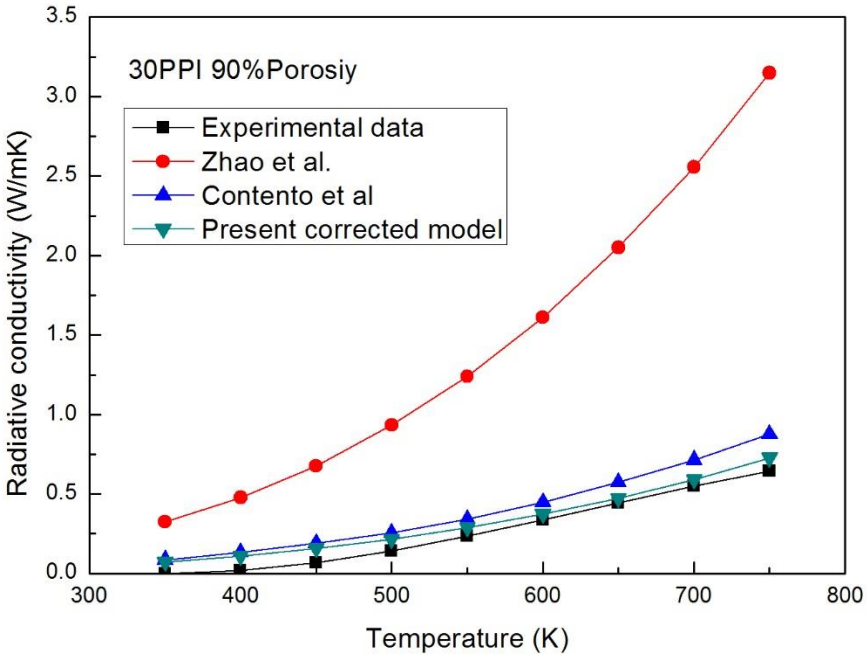

519

520 **Fig. 9.** Comparison between predicted results of present corrected model and
521 experimental data, results of previous 3D models for S2.

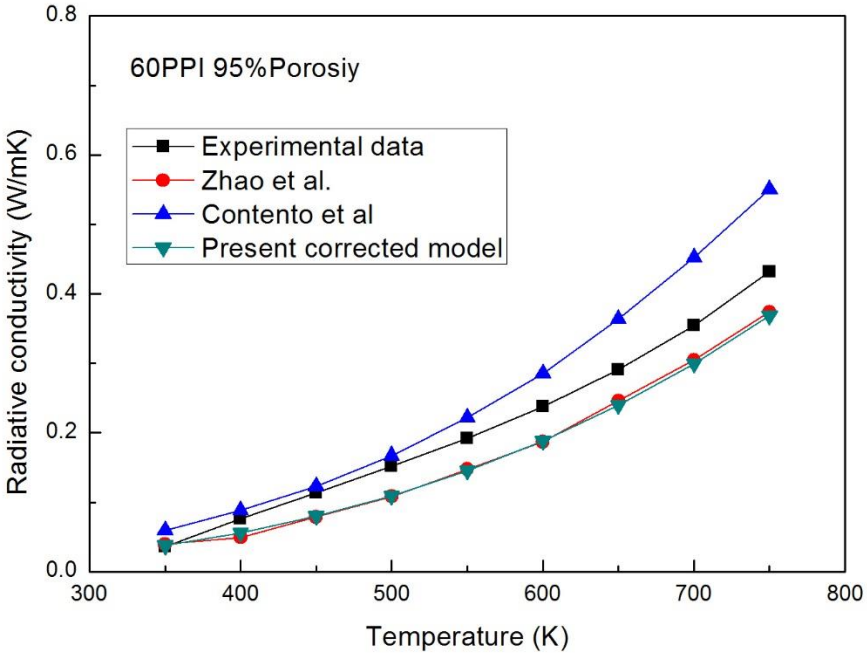

522

523 **Fig. 10.** Comparison between predicted results of present corrected model and
524 experimental data, results of previous 3D models for S3.

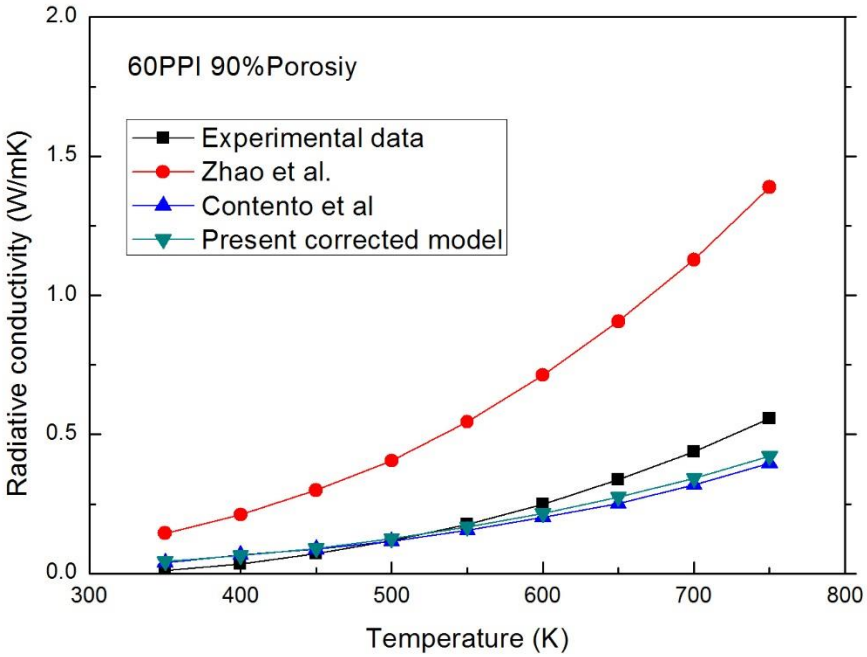

Fig. 11. Comparison between predicted results of present corrected model and experimental data, results of previous 3D models for S4.

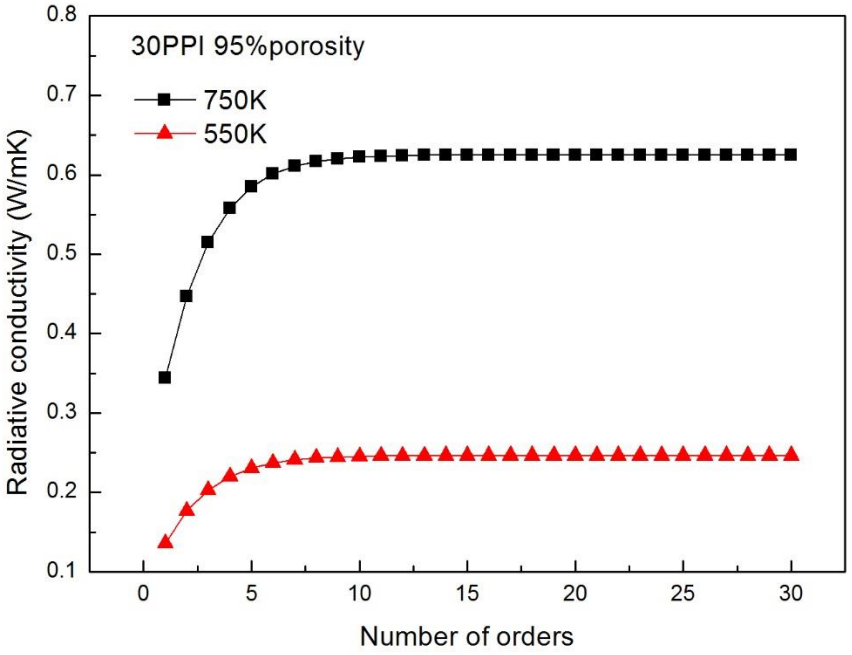

Fig. 12. Radiative conductivity vs. the number of orders at fixed solid emissivity of 0.6 and different temperatures for S1.

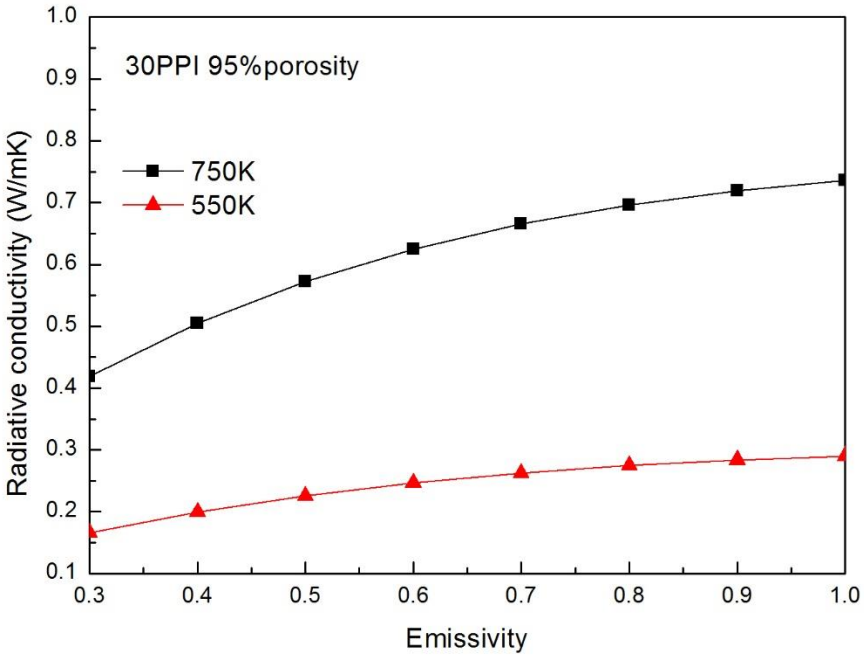

531

532 **Fig. 13.** Radiative conductivity vs. solid emissivity at different temperatures for S1.

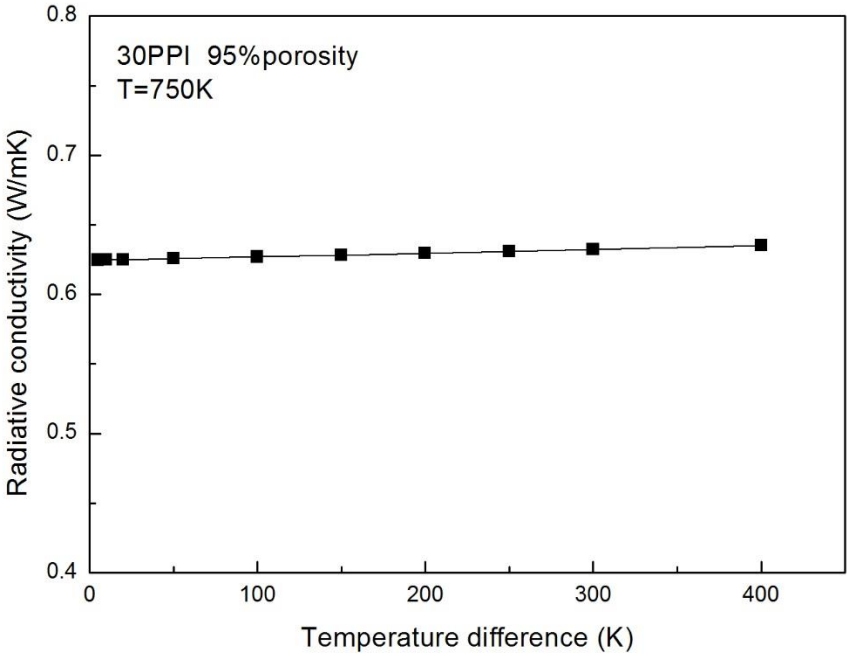

533

534 **Fig. 14.** Radiative conductivity vs. temperature difference at fixed mean temperature
535 for S1.

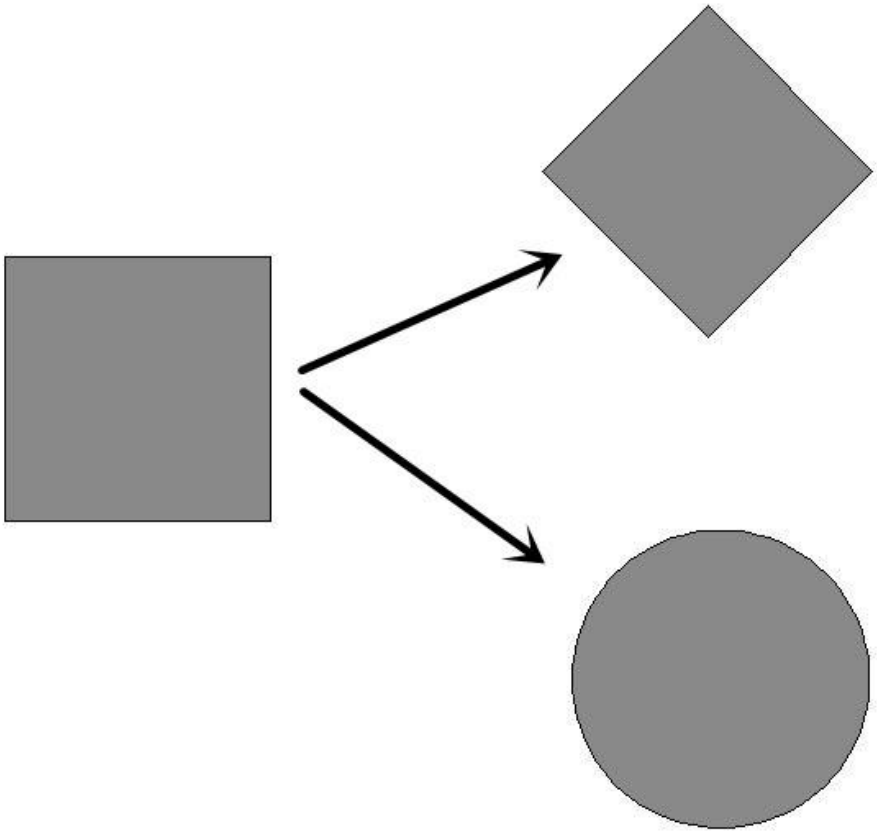

Fig. 15. Different shapes of solid particle.

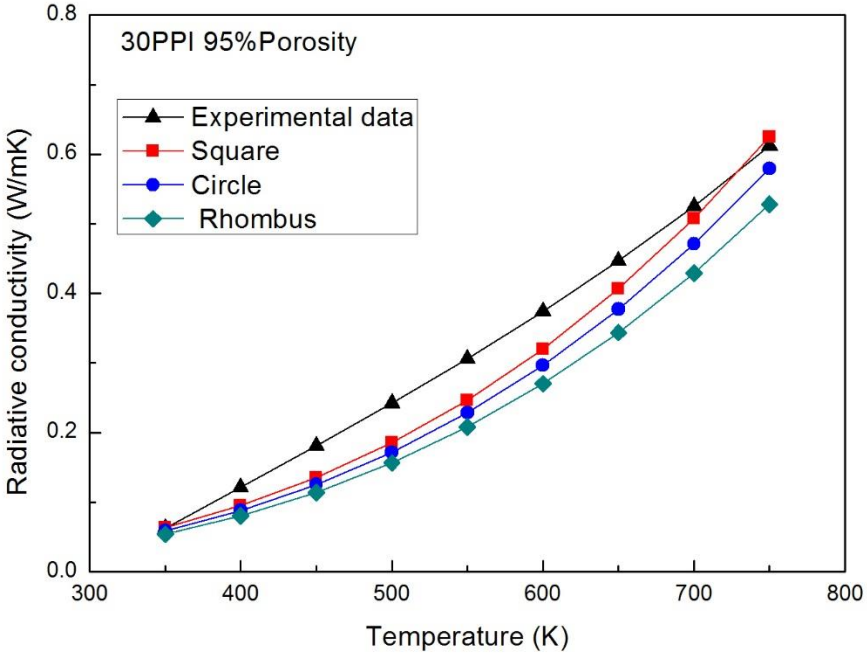

Fig. 16. Effect of shape of solid particle on radiative conductivity for S1.

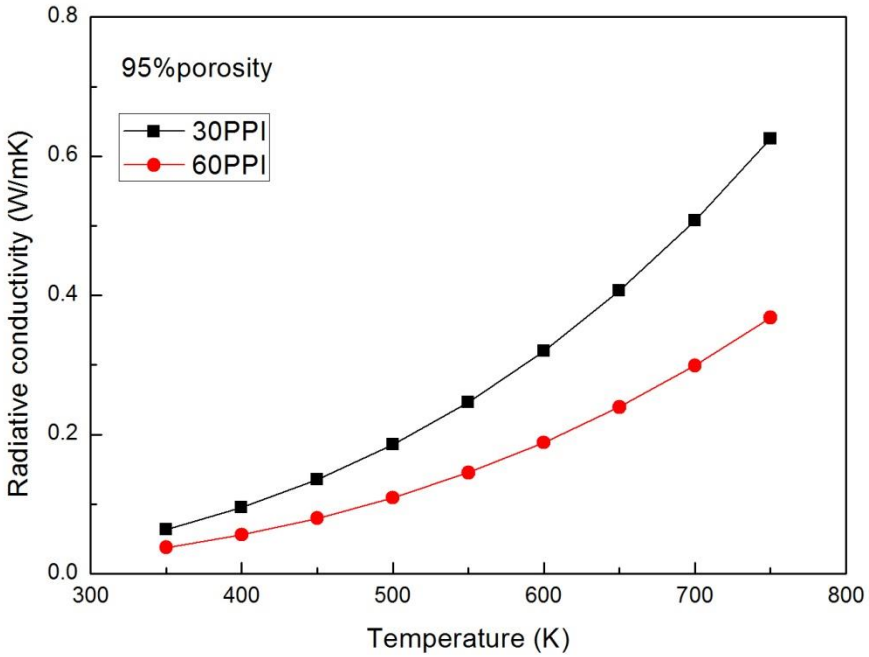

Fig. 17. Radiative conductivity vs. temperature at different PPI.

Table 1

Geometric properties of different foam samples [26].

	Sample			
	S1	S2	S3	S4
Pores per inch (PPI)	30	30	60	60
Nominal porosity (%)	95	90	95	90
Measured porosity (%)	95.9	90.7	94.5	90.8
Nominal cell size(mm)	0.847	0.847	0.423	0.423
Measured cell size(mm)	1.999	2.089	0.975	0.959
Equivalent cell size(mm)	1.772	1.851	0.864	0.850
Measured diameter of the strut(mm)	0.215	0.267	0.124	0.154

Table 2

Percent differences between predicted results and experimental data.

Sample	Zhao et al.'s model [25]	Contento et al.'s model [26]	Present corrected model
S1	-48.16	-17.35	-12.49
S2	485.95	63.37	35.57
S3	-19.14	23.98	-19.23
S4	205.50	-13.17	-7.07